

SHALLOW WATER MODEL FOR ALUMINIUM ELECTROLYSIS CELLS WITH VARIABLE TOP AND BOTTOM

Valdis Bojarevics and Koulis Pericleous

University of Greenwich, School of Computing and Mathematical Sciences,
30 Park Row, London, SE109LS, UK
V.Bojarevics@gre.ac.uk

Keywords: aluminium electrolysis cells, MHD stability, interface waves, shallow layer, dynamic multiphysics modelling

Abstract

The MHD wave instability in commercial cells for electrolytic aluminium production is often described using ‘shallow water’ models. The model [1] is extended for a variable height cathode bottom and anode top to account for realistic cell features. The variable depth of the two fluid layers affects the horizontal current density, the wave development and the stability threshold. Instructive examples for the 500 kA cell are presented.

Introduction

The MHD stability problem for aluminium electrolysis cells is of increasing importance due to significant electrical energy costs, disruptions in the technology and control of environmental pollution rate. The electric current with the associated magnetic field, are intricately involved in the oscillation process and a possible instability of the interface between liquid aluminium and electrolyte. This interaction results in the wave frequency shift from the purely hydrodynamic ones (see [2] and references therein). Moreau and Evans [3] introduced the linear friction model for the wave motion and the horizontal circulation, and attempted to introduce models for the electrolyte side channel effects on the circulation. Actually, the linear friction and the variable bottom effects are used widely in the sea wave theoretical studies [4]. The linear friction is a simplification of the more general nonlinear bottom friction term appearing in the shallow water models, see for example [5].

The systematic perturbation theory for the shallow layer fluid dynamics and, similarly, for the electric current problems, permitting to reduce the three-dimensional problem of the aluminium cell to a two-dimensional shallow layer problem was developed in [6]. This work mathematically proved the wave oscillation frequency shift due to the magnetic interaction and the possibility of a resonant growth. The wave model has been extended to the weakly nonlinear case using the Boussinesq formulation including the linear dispersion terms [7]. The intense turbulence generated by the horizontal circulation velocity is a critical feature to determine the level of damping friction level. A correct damping level permits just a small amplitude self-sustained oscillations observed in real cells, known as ‘MHD noise’. The fully coupled real cell problem requires time dependent, extended electromagnetic field simulation including the fluid layers, the whole bus bar circuit and the ferromagnetic effects [1]. The present paper extends the ‘shallow layer’ theory

and the complete dynamic MHD model to the cases of variable bottom of aluminium pad and the variable thickness of the electrolyte due to the anode nonuniform burn-out process and the presence of the side channels.

Mathematical model for waves at the interface between two liquid shallow layers

The electric current to the individual cell is supplied from above via massive anode bus bars, from which anode rods connect to the carbon anodes. The liquid electrolyte layer beneath the anode blocks is relatively poor electrical conductor of a small depth (4-5 cm) if compared to its horizontal extension (4-5 m in width and 15-20 m in length). The electrolyte density ($\rho_2 = 2.1\text{e}3 \text{ kg/m}^3$) is just slightly lower than the liquid aluminium ($\rho_1 = 2.3\text{e}3 \text{ kg/m}^3$) in the bottom layer of typical depth 15–30 cm. The ‘shallow layer’ approximation assumes that the horizontal dimensions L_x and L_y are much larger than the typical depth H for each of the layers, and, in addition to this, the interface wave amplitude A is assumed to be small relative to the depth H . In the present extension of the theory for a variable layer depth we will assume that the layer deformation is similarly small. Thus the two small parameters of the problem are the nondimensional depth $\delta = H/L_y$ and the amplitude $\varepsilon = A/H$. The resulting fluid dynamic equations become two-dimensional after the depth averaging procedure is applied to the horizontal momentum equations. The equations for the combined horizontal velocity (horizontal circulation \mathbf{u}_0 , plus ε -order $\hat{\mathbf{u}}_\varepsilon$ wave motion) are:

$$\hat{\mathbf{u}} = (\bar{H}_i - \bar{H}_o)^{-1} \int \mathbf{u} d\bar{z} = \mathbf{u}_0 + \varepsilon \hat{\mathbf{u}}_\varepsilon \quad (1)$$

$$\begin{aligned} \rho(\partial_i \hat{u}_j + \hat{u}_k \partial_k \hat{u}_j) = & -\partial_j p(\bar{H}_0) - \varepsilon \partial_j \zeta - \mu \hat{u}_j + \\ & + Re^{-1} \partial_k v_e \partial_k \hat{u}_{0j} + E \hat{f}_j - \frac{1}{2} \delta E \bar{H}_i \partial_j \hat{f}_z, \end{aligned} \quad (2)$$

where the continuity of the pressure at the interface is satisfied by introducing the pressure $p(\bar{H}_0)$ at the common interface

$$\bar{H}_0 = H_0 / (L\delta) = \varepsilon \zeta(x, y, t). \quad (3)$$

The summation convention is assumed over the repeating indexes k (1 or 2, respectively for x, y coordinates). The nondimensional variables are introduced using the following typical scales: $u_0 = \sqrt{gH}$ for the wave velocity; L/\sqrt{gH} for time t , $\rho_1 u_0^2$ for

pressure p , IB_0/L^2 for the electromagnetic force \mathbf{f} (B_0 is typical magnetic field magnitude and I the total electric current), the relative (to Al layer 1) density $\rho = \rho_i/\rho_l$. The nondimensional parameters are the Reynolds number Re and the electromagnetic interaction parameter E :

$$Re = Lu_0/\nu, \quad E = (IB_0/L^2)/(\rho_l u_0^2/L) = IB_0/(L^2 \rho_l g \delta).$$

The effective turbulent viscosity $\nu_e(x,y,t)$ is computed according to the depth averaged versions of empirical turbulence models. For our simulations we used a version of $k-\omega$ two equation model previously validated for various recirculating MHD flows [8]. The nonlinear friction at the top and bottom of the fluid layers in (2) is defined similarly to general shallow water models [5]:

$$\mathbf{Re}^{-1} \delta^{-2} (\bar{H}_i - \bar{H}_o)^{-1} \int \partial_{\bar{z}} \nu_e \partial_{\bar{z}} u_j \, d\bar{z} = C_f |\hat{\mathbf{u}}| \hat{u}_j = \mu \hat{u}_j. \quad (4)$$

The depth averaged continuity equation can be obtained by a similar procedure, giving

$$\varepsilon \partial_i \zeta = \partial_j [(\bar{H}_i - \varepsilon \zeta) \hat{u}_j]. \quad (5)$$

The mathematical solution of the wave problem can be simplified considerably by excluding the velocities and obtaining a single wave equation for the common interface $\zeta(x,y,t)$. This procedure was relatively simple for the case when the bottom and top surfaces were flat [6]: taking the time derivative of (5) and the horizontal divergence of (2). However, for the case of two layers with the variable bottom and top this procedure does not work straightforward. The common pressure $p(H_0)$ at the interface can be eliminated only after the assumption that the top and bottom surfaces are varying sufficiently smoothly to satisfy the condition:

$$\partial_j (\bar{H}_i) = O(\varepsilon). \quad (6)$$

Taking this into account and reverting back (for the final numerical solution purpose) to the dimensional quantities, we have the wave equation for the aluminium-electrolyte interface $H(x,y,t)$ with the variable bottom $H_b(x,y)$ and top $H_t(x,y)$:

$$\begin{aligned} & \left(\frac{\rho_1}{H-H_b} + \frac{\rho_2}{H_t-H} \right) \partial_{tt} H + \left(\frac{\rho_1 \mu_1}{H-H_b} + \frac{\rho_2 \mu_2}{H_t-H} \right) \partial_{tt} H - \\ & - (\rho_1 - \rho_2) g \partial_{jj} H = \\ & = \partial_j (\hat{f}_{j2} - \hat{f}_{j1}) - \frac{1}{2} (H-H_b) \partial_{jj} \hat{f}_{z1} - \\ & - [\rho_1 \partial_j (\hat{u}_{k1} \partial_k \hat{u}_{j1}) - \rho_2 \partial_j (\hat{u}_{k2} \partial_k \hat{u}_{j2})] \end{aligned} \quad (7)$$

The previous linear stability models can be recovered from (7) by excluding the nonlinear horizontal velocity term, the vertical electromagnetic force component f_z contribution, and assuming the H_b and H_t as constants. The nonlinear equation (7) extends the wave description to the weakly nonlinear and slowly varying top and bottom cases.

The horizontal circulation velocities, driven by the rotational part of the electromagnetic force, can be calculated by solving the

equation (2) in the two layers. The numerically efficient procedure consists of taking first the curl of the equation (2), then to rewrite it for the two-dimensional horizontal flow stream function. The solution of the resulting 4th order equation for the stream function is sought in combination with the 2-equation turbulence model for the effective viscosity [8].

Electromagnetic problem

Since the magnetohydrodynamic driving force is $\mathbf{f} = \mathbf{j} \times \mathbf{B}$, the electric current distribution, particularly the horizontal components, are equally important to the magnetic field optimization. Physical and engineering considerations suggest that both problems are mutually interconnected and should be solved interactively. It means that the computer program can use the same data input to compute the electric current, voltages, temperatures in the bus network, the magnetic field, the current distribution within the cell with waving metal interface, then finally iterate back to account for the spatially and temporally variable cell interpolator distance and the effect on the current distribution in the supplying bus network. This affects also the magnetic field, the metal pad waves, velocities, and the neighbor cells which are interconnected to the particular test cell.

The electric current distribution is calculated by coupling the electric current in the fluid zone to the resistance network representing the elements of individual anodes and cathode collector bars, as well as the whole bus-bar circuit between two adjacent cells. The electric current in the fluid zones is computed from the continuous media equations governing the DC current (which can change in time with the waves and anode burnout process):

$$\mathbf{j} = -\sigma \nabla \varphi + \sigma \mathbf{v} \times \mathbf{B}, \quad (8)$$

where the fluid flow induced currents are accounted only in the highly conducting liquid aluminium. The electric potential in the fluid is governed by the equation:

$$\nabla^2 \varphi = \nabla \cdot (\mathbf{v} \times \mathbf{B}), \quad (9)$$

and the boundary conditions of zero current at the insulating walls, given current distribution \mathbf{j}_a at anodes, \mathbf{j}_c at cathode carbon. \mathbf{j}_a and \mathbf{j}_c are obtained from the linear element resistivity network solution, which in turn is coupled to the computed potential distribution from the equation (9). At the interface between the liquid metal and the electrolyte the continuity of the potential and the electric current normal component must be satisfied.

Since the depths of the liquid layers are extremely small if compared to their horizontal extension, the shallow layer approximation is very efficient to solve this 3-dimensional problem. The solution, for instance in the aluminium layer, can be obtained from the following equation:

$$\begin{aligned} & j_{za}(x, y, t) - j_{zc}(x, y, t) = \\ & \sigma_{Al} \partial_k ((H(x, y, t) - H_b(x, y)) \partial_k \varphi), \end{aligned} \quad (9)$$

where the aluminium interface $H(x,y,t)$ and the bottom are variable. The current distribution at the top and the bottom depend on the iterative solution from the linear element network of the bus bars, anodes, pins, collector bars, etc.

Magnetic field in an aluminium cell is created by the currents in the cell itself and from the complex bus-bar arrangement around the cell, in the neighboring cells and the return line, and by the effect of cell construction steel magnetization. The complexity of any practically usable magnetohydrodynamic (MHD) model of the cell arises from the coupling of the various physical effects: fluid dynamics, electric current distribution, magnetic field and thermal field. The MHD model presented here accounts for the time dependent coupling of the current and magnetic fields with the bath-metal interface movement. The magnetic field from the currents in the full bus-bar network is recalculated at each time step during the dynamic simulation using the Biot-Savart law. A very similar technique is used on the 3D grid within the cell fluid layers where a special analytical technique is applied to deal with the singularity in the Biot-Savart law in order to obtain a smooth and converging solution.

500 kA demonstration cell

The numerical solution of the described MHD model uses a relatively coarse mesh of $64 \times 32 \times 2$ and a smooth spectral function representation in the space of each fluid layer. This ensures a good accuracy solution and enables one to re-compute the electromagnetic and fluid dynamic field time dependent distribution in a reasonable computational time. The solution is sufficiently smooth because of the global pseudo-spectral approximation used for the velocity and interface discretisation, which permits much higher accuracy in comparison to finite element or finite volume approximations on the similar grid size.

The aluminium-electrolyte interface and the variable electrolyte top makes the anode currents unequal because of the local ACD change. The model includes an option to account for the time average gradual consumption of the anode bottom to conform to the ACD change. An artificially accelerated anode burn-out is permitted in order to achieve the result in a reasonable computational time interval. The importance of this option was already demonstrated in the recent study [1], demonstrating a significant stabilization effect.

The present model includes the ability to prescribe the variable bottom and top of the cell, and permits to investigate the effects on the cell MHD stability. There are two new physical effects: the wave propagation in the variable depth layer is changed, and the horizontal component of the electric current is increased in the narrow part of the layer. The second effect can alter the MHD stability.

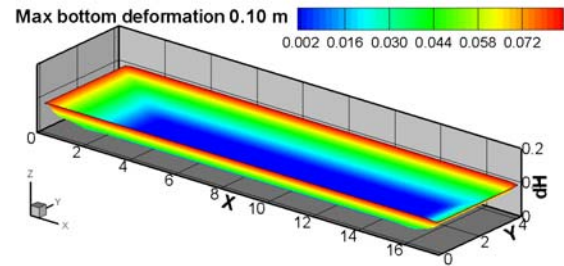


Figure 1. Metal pad bottom shape (concave).

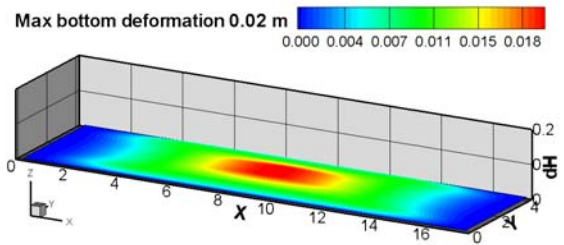


Figure 2. Metal pad bottom shape (convex).

Let us consider some examples of the new model application. Quite often the cavity of the electrolysis cell is not simply a rectangular box, but instead has sloping bottom of a concave shape. Figure 1 shows the bottom profile used in some test runs. An another type of bottom used in our tests is the convex deformation shown in the Figure 2. The top surface of the electrolyte is facing the immersed anode, which is often of non-uniform bottom profile. Additionally the side channels can be of importance for the waves and currents. The example of the interpolated anode bottom and the side channels is shown in the Figure 3.

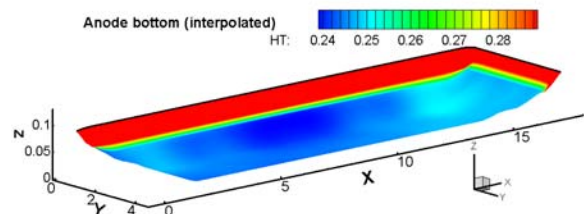


Figure 3. The anode bottom and side channels profile used in the test runs

Firstly, we would like to test the simplest case of pure gravity waves in the cell of variable bottom and top for the present two fluid case. When using the bottom profile shown in the Figure 1 and the top from figure 3, the resulting wave behavior is shown in the Figure 4. The first gravity mode (1,0) wave in the rectangular

box is shown for reference. The presence of the variable bottom only, makes little change on the wave shape, just slight increase of the wave period can be detected because the average depth is reduced. However, when adding the effect of the top side channels, the wave amplitude starts to decrease gradually. The change of the shape of the gravity waves for different bottom is illustrated in the Figure 5.

The full MHD interaction cases are more complex because of the multiple physical effects being coupled. The figure 6 shows the interface shape at a particular time moment at 500 s from the start of simulation, and the Figure 7 demonstrates the oscillation pattern compared with the previous software and the present update accounting for the variable coefficients wave equation. The comparison is done for the flat bottom case, and it gives an evidence that the different numerical solver (more complex and slower) is giving practically identical results to the previous.

The Figure 8 presents the interface shape for the case when the bottom profile is variable (corresponding to the Figure 1, concave). It looks rather similar in shape, yet the amplitudes are different, as can be seen from the figure 9. The oscillation frequency is also slightly shifted.

The largest difference can be observed when the top surface of the liquid electrolyte is subject to the variation as well (Figures 10 and 11). The amplitudes has grown and the frequency shift is even more noticeable.

The most sensitive parameter for the bottom and top variation effect can be detected by comparing the electric current distribution in the aluminium layer. The Figures 12 and 13 give evidence to the change in the J_y electric current component, which is the most important parameter for any stability theory of the aluminium cells. The concave bottom case leads to the increased horizontal current density at the ends of the cell, what makes the electromagnetic interaction with the B_z magnetic field more pronounced, particularly because the B_z field is usually the worst in the vicinity of the corners.

The J_x current component in the metal is affected as well, however to a lesser amount (Figures 14 and 15). The J_z at the bottom (Figure 16) is mostly influenced by the presence of nonconducting ledge (included in the present model [9]), and the vertical elevation of the bottom is less important.

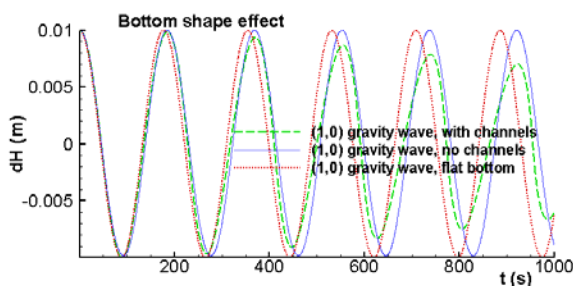


Figure 4. The gravity wave (1,0) variation with the top and bottom.

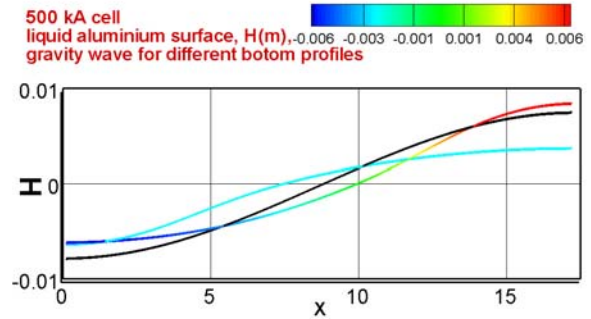


Figure 5. The gravity wave shape for different bottoms: flat, concave, concave nonsymmetrical.

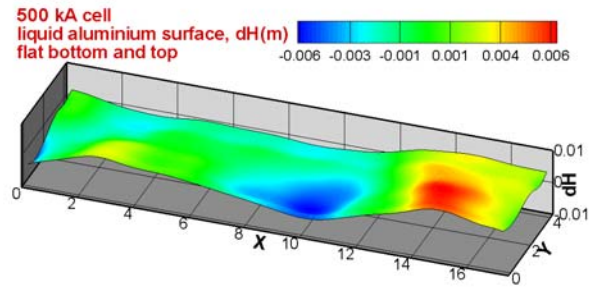


Figure 6. The interface shape at 500s for the flat bottom.

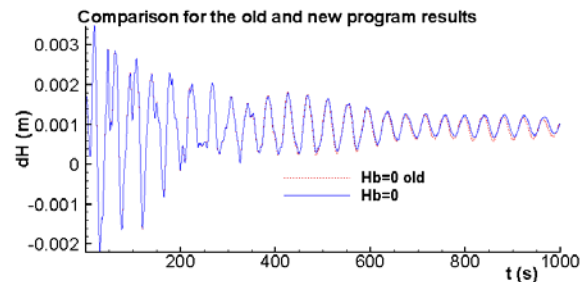


Figure 7. Oscillation pattern: the comparison of the 500 kA demonstration cell test results before and after the variable bottom upgrade.

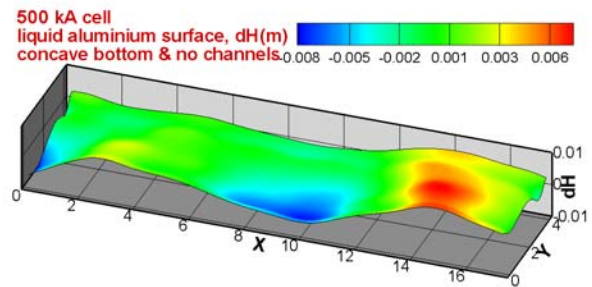


Figure 8. The interface shape at 500s for the concave shaped bottom, but not including the electrolyte channel effect.

Additionally we would like to point out that the present MHD model is coupling together all magnetic and electrical fields at all times of the wave evolution. If the magnetic field is not precisely coupled to the small variations of the electric current due to the waves, then the cell can be wrongly diagnosed as being unstable, as it is demonstrated in the Figure 17. There is a significant shift in the frequency and this is well known to be the source of the MHD instability in the aluminium electrolysis cells. The possibility to modulate the magnetic field to a proper frequency by external means could be a possibility to either enhance the cell stability or to reduce it and make the cell a failure for practical use. The software presented here can be used to detect such effects and to choose the favorable adjustments.

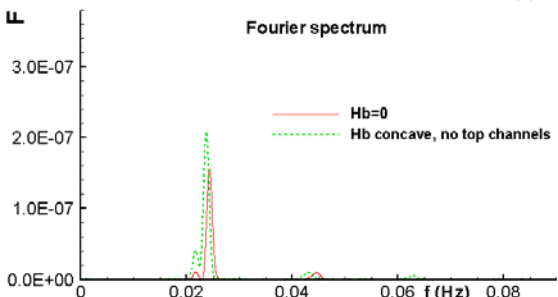
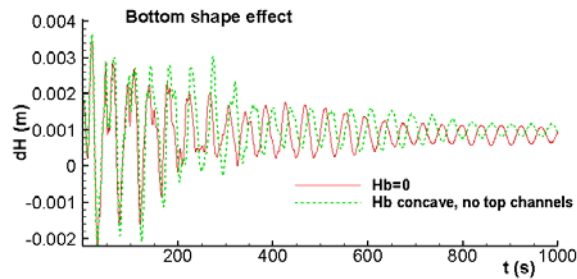


Figure 9. Oscillation pattern: the comparison of the flat and concave shaped bottom not including the electrolyte channel effect.

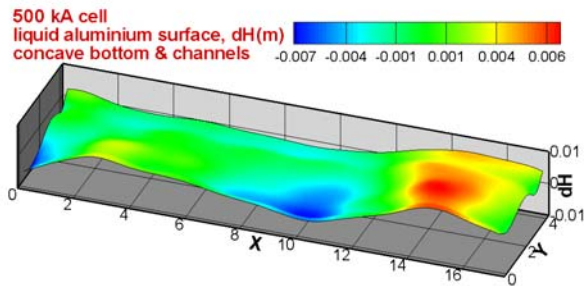


Figure 10. The interface shape at 500s for the concave shaped bottom including the electrolyte channels effect.

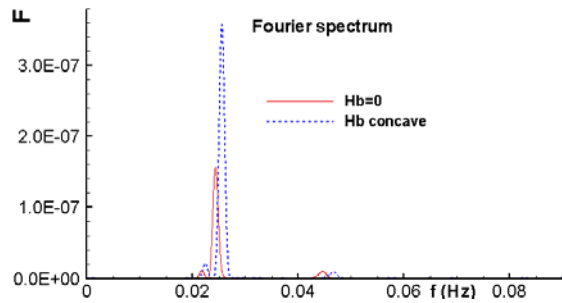
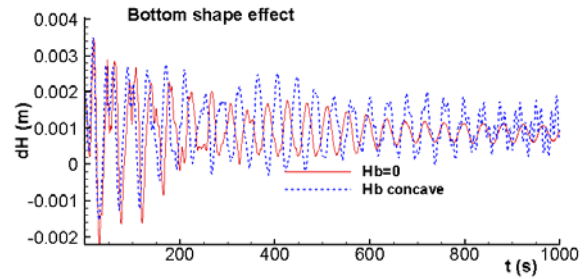


Figure 11. Oscillation pattern: the comparison of the flat and concave shaped bottom including the electrolyte channel effect.

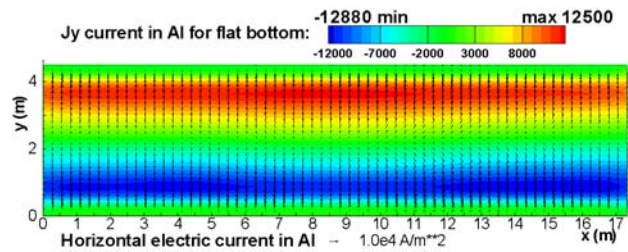


Figure 12. The horizontal electric current J_y in the metal pad for the flat bottom case.

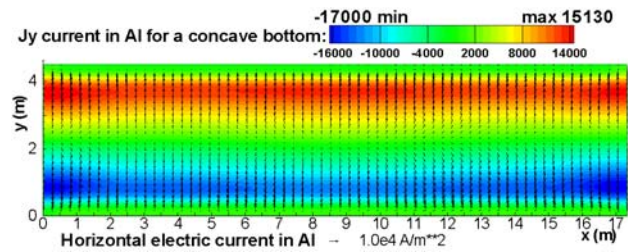


Figure 13. The horizontal electric current J_y in the metal pad for the concave bottom case.

Conclusions

MHD model for the non-linear cell stability analysis software was updated to take into account the deformed bottom and top surfaces of the cell cavity.

For the 500 kA demonstration cell, the non-linear cell stability analysis results show that the bottom deformation affects the cell stability. The presence of the electrolyte channels and the anode bottom deviation from flat is of even more pronounced effect.

The most sensitive reaction is to the change in the horizontal current J_y component in the liquid metal.

The magnetic field updating during the cell dynamic wave development is of high importance to predict the stability threshold.

References

1. V. Bojarevics and K. Pericleous, "Comparison of MHD Models for Aluminium Reduction Cells". *In Proceedings of TMS Light Metals* (2006), 347-352.
2. R. Von Kaenel and J.P. Antille. Magneto-hydrodynamic stability in alumina reduction cells. *Travaux*, 23 (1996), no. 27, 285-297.
3. R. Moreau and J.W. Ewans. An analysis of the hydrodynamics of aluminium reduction cells. *Journal of Electrochemical Society*, 131 (1984), no. 10, 2251-2259.
4. C. C. Mei. *The Applied Dynamics of Ocean Surface Waves* (World Scientific, 1989).
5. A.K. Rastogi and W. Rodi. Prediction of heat and mass transfer in open channels. *J. Hydraulics Division ASCE*, HY3 (1978), 397-420.
6. V. Bojarevics and M. V. Romerio. Long waves instability of liquid metal-electrolyte interface in aluminium electrolysis cells: a generalization of Sele's criterion. *Eur. J. Mech., B/Fluids*, 13 (1994), no 1, 33-56.
7. V. Bojarevics. Nonlinear waves with electromagnetic interaction in aluminium electrolysis cells. *Progr. Fluid Flow Res.: Turbulence and Applied MHD. AIAA* (1998), Chapter 58, 833-848.
8. V. Bojarevics, K. Pericleous, R.A. Harding and M. Wickins. The Development and Validation of a Numerical Model of an Induction Skull Melting Furnace. *Metallurgical and Materials Transactions*, 35B (2004), 785-803
9. M. Dupuis and V. Bojarevics. Weakly coupled thermo-electric and MHD mathematical models of an aluminium electrolysis cell. *In Proceedings of TMS Light Metals* (2005), 449-454.

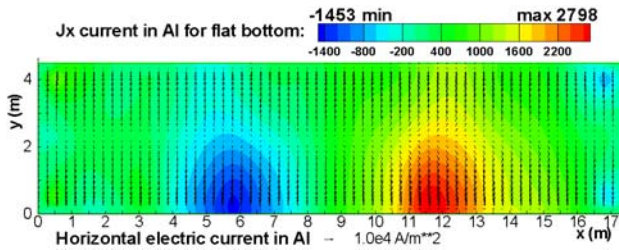


Figure 14. The horizontal electric current J_x in the metal pad for the flat bottom case.

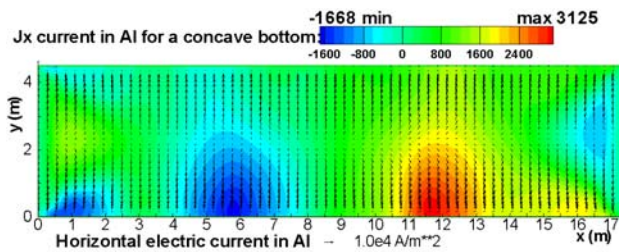


Figure 15. The horizontal electric current J_x in the metal pad for the concave bottom case.

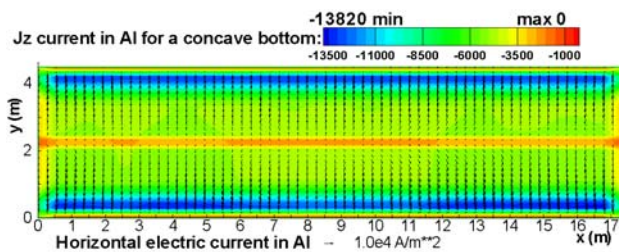


Figure 16. The horizontal and vertical electric current J_z in the metal pad for the concave bottom case.

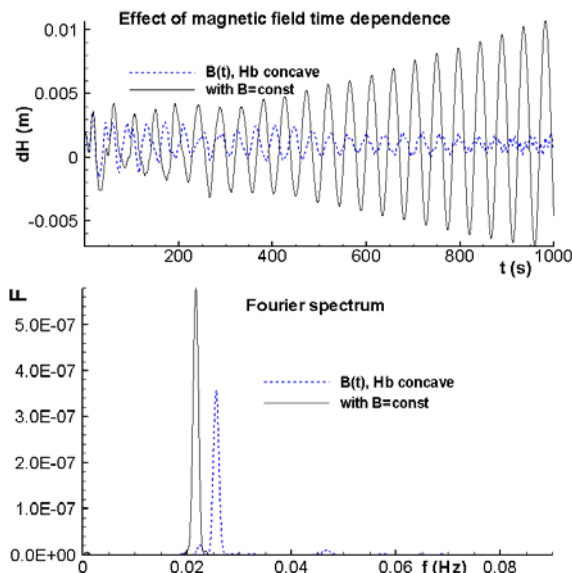


Figure 17. Oscillation pattern: the comparison for the magnetic field time dependence of the concave shaped bottom case including the electrolyte channels effect.